ORGANOMETALLICS

Article

pubs.acs.org/Organometallics

Cyclometalated Platinum(II) Complexes Bearing Bidentate *O,O′*-Di(alkyl)dithiophosphate Ligands: Photoluminescence and Cytotoxic Properties

Masood Fereidoonnezhad,[†,‡] Babak Kaboudin,[§] Tabassom Mirzaee,[†] Reza Babadi Aghakhanpour,[§] Mohsen Golbon Haghighi,[∥] Zeinab Faghih,[⊥] Zahra Faghih,[#] Zohreh Ahmadipour,[†] Behrouz Notash,[∥] and Hamid R. Shahsavari*[,§]

[†]Department of Medicinal Chemistry, School of Pharmacy and [‡]Cancer, Environmental and Petroleum Pollutants Research Center, Ahvaz Jundishapur University of Medical Sciences, Ahvaz 61357-15794, Iran

[§]Department of Chemistry, Institute for Advanced Studies in Basic Sciences (IASBS), Yousef Sobouti Boulevard, Zanjan 45137-6731, Iran

[∥]Department of Chemistry, Shahid Beheshti University, Evin, Tehran 19839-69411, Iran

[⊥]Pharmaceutical Sciences Research Center and [#]Shiraz Institute for Cancer Research, School of Medicine, Shiraz University of Medical Sciences, Shiraz 71348-14336, Iran

Supporting Information

ABSTRACT: Mononuclear complexes [Pt(ppy)(S^S)] (**1a**, S^S = *O,O′*-di(cyclohexyl)dithiophosphate (ctp); **2a**, S^S = *O,O′*-di(butyl)dithiophosphate (btp)) and [Pt(bzq)(S^S)] (**1b**, S^S = ctp; **2b**, S^S = btp) have been prepared by the reaction of precursor complexes [Pt(C^N)Cl(dmso)], C^N = deprotonated form of 2-phenylpyrdine (ppy) and 7,8-benzoquinoline (bzq), and potassium salt of S^S ligands. All complexes were characterized by NMR spectroscopy, and the structure of **2b** was further identified by single crystal X-ray determination. Although the complexes are not luminescent in solution at ambient temperature, they become strong emissive materials (bright green) in solid state (at room temperature) with high quantum yields and long lifetimes in the microsecond domain. In frozen glass state or at low temperature (solid state), these complexes become better emissive in relation to room temperature. UV−vis spectra, supported by TD-DFT calculations, indicate that ^{1}ILCT (intraligand charge transfer) predominates over the other transitions (L = C^N cyclometalated ligand). Accordingly, **1** and **2** exhibit structured emission bands which display a large involvement of ^{3}LCCT (ligand-centered charge transfer) with lower contribution of ^{3}MLCT (metal to ligand charge transfer) transition in the excited states. Also, biological activities of **1** and **2** were evaluated against three human cancer cell lines including A549 (human lung cancer), SKOV3 (human ovarian cancer), and MCF-7 (human breast cancer). **2a** presented an effective potent cytotoxic activity regarding to the cell lines. The cellular localization of **1a** and **2a** in MCF-7 human cells was investigated by fluorescence microscopy.

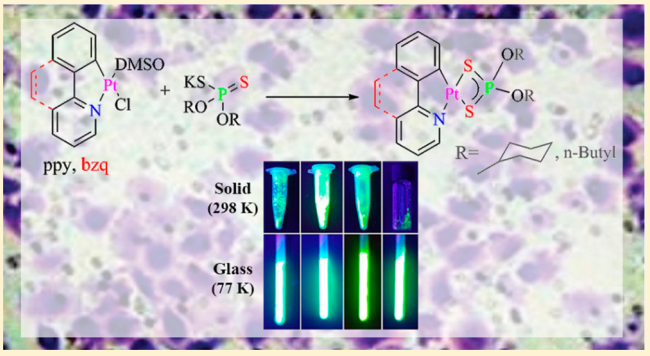

INTRODUCTION

Heteroleptic cycloplatinated(II) complexes incorporating appropriate ancillary ligands represent impressive photophysical properties.[1−9] Also, they have wide range of applications regarding these properties such as light-emitting devices,[9,10] photocatalytic processes and hydrogen generation,[11] dye-sensitized solar cells,[12] biosensors, and photoswitches.[13−15] A key step in the design of such emissive complexes can be picking out suitable ancillary ligands.[16] In recent years, the ancillary chelating L^X systems have been developed in order to tune and enhance the emission properties of the cycloplatinated(II) complexes; they are also able to impose an extra structural rigidity on the complex.[17] This kind of ligand is the combination of a neutral L ligand and an anionic X head. Some anionic O^O, N^N, and N^O chelates have been employed as the successful examples of L^X ancillary ligands toward the cyclometalated complexes.[16,18−23] Phosphino alcohols can also give a special puckered P^O ancillary ligand in which the phosphorus head can play role of a strong-field ligand with π-accepting character.[24] Although the use of L^X ancillary ligands in the structure of cycloplatinated(II) complexes is widespread in the literature,[2,6,16,25,26] such complexes bearing S^S chelating systems[27,28] like dithiocarba-

Received: January 22, 2017

DOI: 10.1021/acs.organomet.7b00054
Organometallics XXXX, XXX, XXX−XXX

mates[29] or dithiophosphates[30,31] ligands are scarce in the published resources.

In contrast, *O,O′*-di(alkyl)dithiophosphate ligands[32] (S^S) represent a relatively new class of potentially L^X chelating systems (in cycloplatinated complexes)[30,31] which can be easily obtained by deprotonation of *O,O′*-di(alkyl)dithiophosphoric acid organic compounds.[32] Deprotonation reaction from the acidic species gives the corresponding anion that they can be defined by two resonance forms (Scheme 1). Furthermore, they

Scheme 1. Two Resonance Forms of Deprotonated *O,O′*-Di(alkyl)dithiophosphoric Acid Compounds

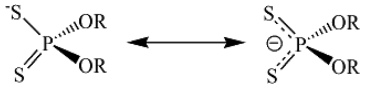

exhibit various coordination patterns toward a wide range of metal ions[33] while some binding modes are typically shown in Scheme 2.[32] For instance, the soft metals such as platinum prefer to bind the structure "**b**" for producing isobidentate coordination pattern (**4**).[30−33]

Scheme 2. Diversity of Coordination Patterns of *O,O′*-Di(alkyl)dithiophosphate Ligands toward Different Metal Ions

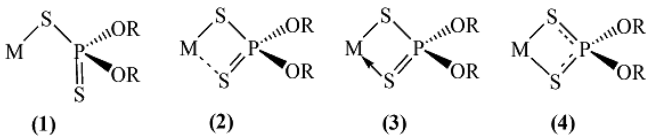

In the present study, a new series of cyclometalated platinum(II) complexes containing *O,O′*-di(alkyl)dithiophosphates (alkyl = cyclohexyl and *n*-butyl) were synthesized and characterized spectroscopically. Due to the lack of perfect investigations on the cycloplatinated(II) complexes containing S^S ligands, we have decided to study the effect of such ancillary ligands on the luminescence and biological properties of these Pt(II) complexes. Additionally, the obtained photoluminescence data was supported by density functional theory (DFT) and time-dependent DFT (TD-DFT) calculations. Also, the cytotoxic activities of platinum complexes comprising S^S ligands have been evaluated against three cancer cell lines, i.e., A549 (human lung cancer), SKOV3 (human ovarian cancer), and MCF-7 (human breast cancer). Moreover, as these complexes are intensely emissive, their cellular localization was studied by fluorescence microscopy.

RESULTS AND DISCUSSIONS

Synthesis and Characterization of Complexes. The new chemistry is depicted in Scheme 3. The well-known precursor complexes [Pt(C^N) (Cl) (dmso)],[34,35] where C^N = deprotonated form of 2-phenylpyridine (ppy) and 7,8-benzoquinoline (bzq), were treated with 1 equiv of different potassium *O,O′*-di(alkyl)dithiophosphate salts (*O,O′*-di(cyclohexyl)dithiophosphate (ctp) and *O,O′*-di(butyl)-dithiophosphate (btp)) and gave corresponding complexes [Pt(ppy)(S^S)] (**1a**, S^S = ctp; **2a**, S^S = btp) or [Pt(bzq)-(S^S)] (**1b**, S^S = ctp; **2b**, S^S = btp).

Complexes **1** and **2** were deduced from common analytical methods such as elemental analyses and mass spectroscopy, and

Scheme 3. Synthetic Route for Preparation of 1 and 2[a]

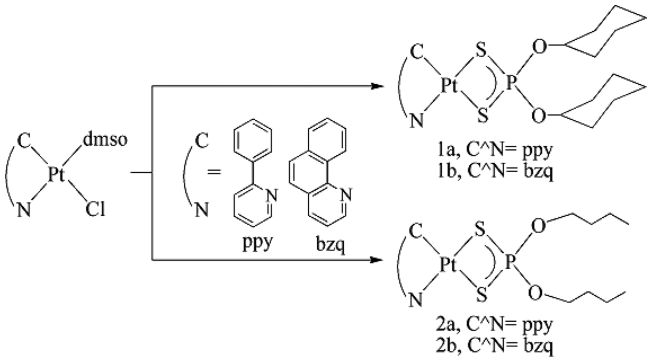

[a]All reactions were carried out under inert atmosphere at room temperature.

their integrity in solid and solution were investigated by IR and NMR spectroscopy, respectively. The details are given in the Experimental Section. The ESI(+) mass spectra (Figure S1−S4) of these complexes reveal the molecular peaks related to $[M]^+$ fragments, which obviously establish **1** and **2** in the gas phase.

IR spectra of **1** and **2** (Figures S5−S8) displayed a strong band due to $\upsilon_{P=S}$ in the region 683−737 cm^{-1} while it shifted to lower frequency ∼30 cm^{-1} with respect to salt ligands. Also, the bands observed in the region of 459−540 cm^{-1} are attributed to υ_{P-S} as symmetric and asymmetric vibrations.

NMR (^1H, $^{31}P\{H\}$) spectroscopy was employed to precisely identify the new structures in solution. The Experimental Section provides the numerical NMR data, while the spectra are embedded in Figures S9−S16. **2a** was typically selected to interpret NMR spectra. In the ^1H NMR spectrum of **2a**, at δ = 0.94 ppm a triplet signal is observed for the terminal methyl of the butyl chains (H^d). Two multiplet signals appearing at δ = 1.44 and 1.74 ppm are related to H^c and H^b protons of the butyl chains, respectively. Also, the signals for two diastereotopic protons of CH_2 groups adjacent to oxygen atoms (H^a) are significantly deshielded and appeared as two triplet signals at δ = 4.21 and 4.23 ppm. In the aromatic region, a distinctive doublet signal being flanked by platinum satellites is observed at δ = 8.79 ppm which corresponded to the H^2 of ppy ligand ($^3J_{HH}$ = 5.7 Hz, $^3J_{PtH}$ = 43.4 Hz). Moreover, the $^{31}P\{H\}$NMR spectrum of **2a** includes a singlet with platinum satellites at δ = 100.8 ppm with $^2J_{PtP}$ = 320 Hz. This coupling constant is relevant to the chelating binding mode of *O,O′*-di(alkyl)-dithiophosphate ligands.[30,36]

Using slow layer diffusion of *n*-hexane into the acetone solution of **2b**, yellow crystals were obtained and provided a good quality for single crystal X-ray crystallography. This complex crystallizes in the monoclinic crystal system with the *P*21/*n* space group. An ORTEP view of **2b** is given in Figure 1 (possessing atom numbering for the important atoms). In this structure, one of the butyl chains is located perpendicular to the molecule plane, while another one is almost parallel to the molecule plan (Figure 1). The four-membered "PtSPS" ring exhibits a puckered structure with an almost tetrahedral geometry at the phosphorus atom center.[30,31] On the basis of the previous experiences, the C^N bite angle is considerably smaller than 90° (83.7°) which proves that the C^N chelate is under a strain.[37,38]

Photophysical Properties. The UV−vis spectra of **1** and **2** in CH_2Cl_2 solutions at room temperature are represented in

DOI: 10.1021/acs.organomet.7b00054
Organometallics XXXX, XXX, XXX−XXX

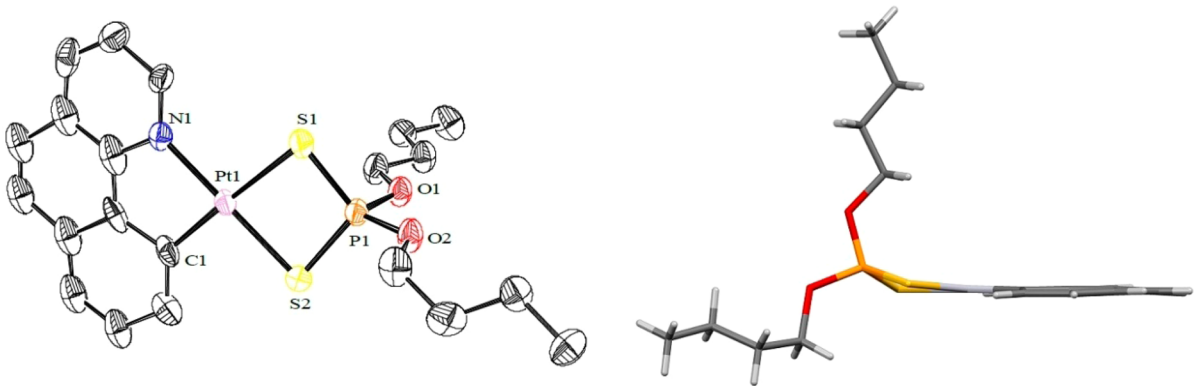

Figure 1. ORTEP plot of the structure of **2b**. Selected geometrical parameters (Å, deg): Pt1−C1 1.980(11); Pt1−N1 2.038(8); Pt1−S1 2.436 (3); Pt1−S2 2.311(3); P1−S1 1.994(4); P1−S2 2.006(4); P1−O1 1.566(8); P1−O2 1.573(8); C1−Pt1−N1 83.7(4); C1−Pt1−S2 94.4(4); N1−Pt1−S2 176.8(3); C1−Pt1−S1 177.8(4); N1−Pt1−S1 98.3(3); S2−Pt1−S1 83.64(10); S(1)−P(1)−S(2) 104.70(17). Ellipsoids are drawn at the 40% probability level, and hydrogen atoms are omitted for clarity.

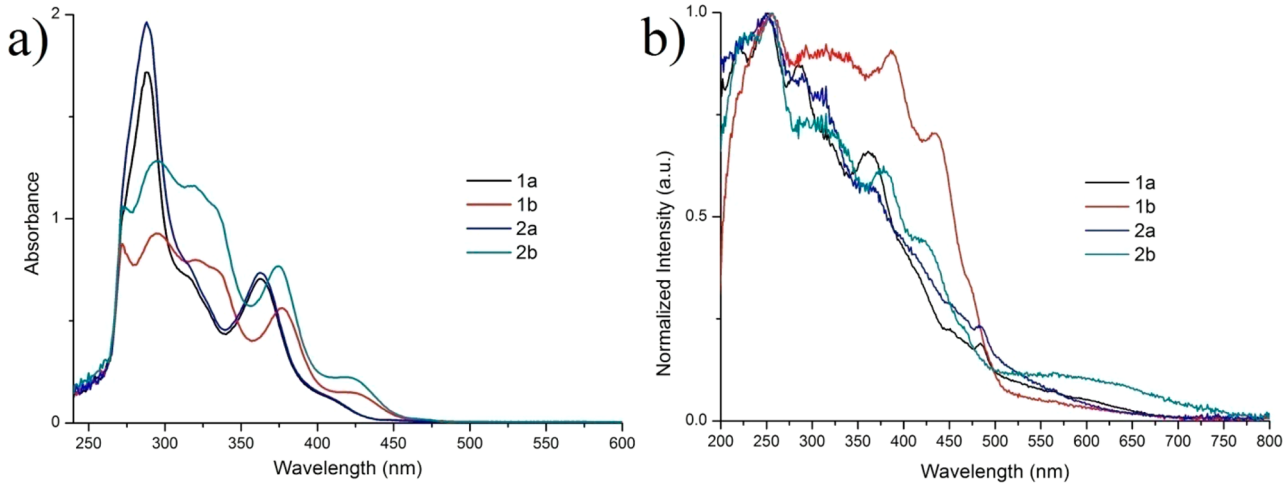

Figure 2. (a) Absorption spectra for **1** and **2** in CH_2Cl_2 solutions. (b) Normalized diffuse reflectance UV−vis spectra of **1** and **2** in solid state at room temperature.

Figure 2a, while their corresponding normalized diffuse reflectance UV−vis spectra are depicted in Figure 2b. The numerical data are listed in Table 1. The UV−vis spectra of complexes in solution bearing the same C^N cyclometalated ligands are almost identical. It indicates that the absorptions do not depend on the nature of alkyl groups in the structure of *O*,*O*′-di(alkyl)dithiophosphate ligands. On the basis of reported assignments for the Pt(II) complexes incorporating C^N aromatic rings,[9,39−41] it is rational to assign the high-energy absorption bands below 350 nm to the ligand-centered (^{1}LC $\pi-\pi^*$) transitions which are perturbed by the metal center. This results in the free ppyH and bzqH compounds showing a ^{1}LC transition lower than 300 nm under the same conditions.[6,42] However, the less intense bands (λ > 350 nm) are normally related to the spin-allowed metal to ligand charge transfer transitions (^{1}MLCT) or the mixture of ^{1}MLCT and ^{1}LC. The bzq complexes (**1b** and **2b**) exhibiting a more extended aromaticity have a redshift in the ^{1}MLCT/^{1}LC region with respect to those of ppy complexes (**1a** and **1b**) which is due to lowering the π^* energy level.[43,44] In the diffuse reflectance spectra of complexes, an overall redshift is observed for the bzq complexes in comparison to the ppy complexes, mirroring the obtained spectra in solution. Almost, there is no observable change between the solid state diffuse reflectance UV−vis spectra and the spectra obtained in solution state which is due to the lack of Pt−Pt or excimeric $\pi-\pi$ interactions.[44] For **2b**, in the low-energy bands, a weak absorption is observed at approximately 580 nm, probably not enough to change the color of this complex.

Table 1. Numerical Absorption Data for 1 and 2 in Their CH_2Cl_2 Solutions (5×10^{-5} M) and Solid State at Room Temperature[a]

complex	absorption (nm (10^4 ε/M^{-1} cm^{-1}))
1a	407 (0.062), 362 (0.351), 313 (0.365), 287 (0.864); CH_2Cl_2
	413, 362, 285, 254; solid
1b	430 (0.068), 377 (0.287), 322 (0.408), 294 (0.470), 271 (0.438); CH_2Cl_2
	437, 388, 321, 253; solid
2a	407 (0.062), 362 (0.372), 313 (0.413), 287 (0.984); CH_2Cl_2
	411, 365, 309, 253; solid
2b	423 (0.112), 374 (0.389), 319 (0.587), 294 (0.649), 271 (0.533); CH_2Cl_2
	425, 375, 310, 254; solid

[a]Data at high concentration (10^{-3} M) are similar to those at low concentration.

DOI: 10.1021/acs.organomet.7b00054
Organometallics XXXX, XXX, XXX−XXX

All complexes exhibit poor and negligible emissions in their CH_2Cl_2 solutions at room temperature because of molecular motions in solution. Conversely, with the exception of **2b**, they are strong green emitters in solid state at room temperature under irradiation of UV light (365 nm) as evidenced by high measured quantum efficiencies (Figure 3 for the corresponding

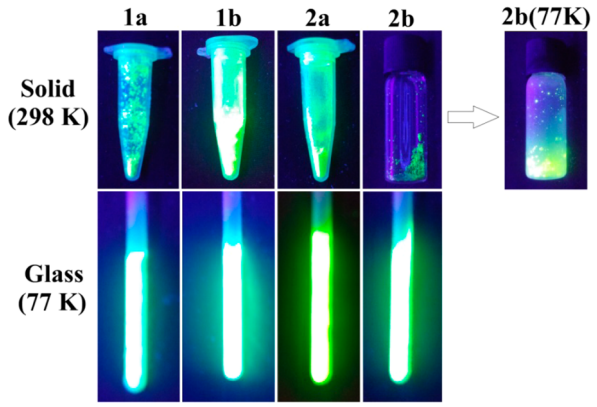

Figure 3. Photographic images of **1** and **2** under UV light in solid and glass states.

photographic images). Expectedly, low temperature (77 K) makes these complexes to display much brighter green luminescence rather than room temperature, even including **2b** which is a relatively poor luminescent at room temperature. Also, the frozen CH_2Cl_2 solutions of complexes demonstrate very shiny strong emissions under UV light exposure (Figure 3). The characters of emissions are definitely phosphorescence due to the large amount of lifetime values in the microsecond range which were obtained using the emission bands maxima of complexes (Table 2).

The normalized emission spectra for the complexes under different circumstances arising from the excitation wavelength between 340 and 500 nm are demonstrated in Figure 4; the numerical data are summarized in Table 2. For all the complexes, the bands occur in green region with tails to the

Table 2. Numerical Data for the Emission Wavelengths of 1 and 2

complex	λ_{em} (nm)/λ_{ex} (nm)	τ (μs)[b]	Φ[b]
1a	490, 520^{max}, 555^{sh} (340–500), solid (298 K)	8.2	0.721
	488, 520^{max}, 556^{sh} (340–500), solid (77 K)	31.1	0.837
	488^{max}, 517, 555^{sh} (340–500), 5×10^{-5} M (77 K)[a]		
1b	510, 530^{max}, 581^{sh} (340–500), solid (298 K)	6.3	0.677
	503, 530^{max}, 570^{sh} (340–500), solid (77 K)	27.7	0.809
	496^{max}, 533, 577^{sh} (340–500), 5×10^{-5} M (77 K)[a]		
2a	490, 520^{max}, 555^{sh} (340–500), solid (298 K)	9.4	0.518
	488, 520^{max}, 556^{sh} (340–500), solid (77 K)	17.5	0.677
	488^{max}, 517, 555^{sh} (340–500), 5×10^{-5} M (77 K)[a]		
2b	$504{,}530^{max}$, 570^{sh} (340–500), solid (298 K)	3.7	0.211
	493, 520^{max}, 555^{sh} (340–500), solid (77 K)	6.8	0.593
	496^{max}, 533, 577^{sh} (340–500), 5×10^{-5} M (77 K)[a]		

[a]Data at high concentration (10^{-3} M) are similar to those at low concentration. [b]Lifetime and quantum yield were measured as a neat powder.

near yellow region. Neither aggregation nor accordingly excimeric emission is observed in the spectra probably because of the presence of bulky R groups of the S^S ancillary ligands. In solid state at 298 K, the bright green powders of **1a** and **2a**, having the same ppy cyclometalated ligand, give structured emission bands with the same wavelengths. It indicates that R substituents on the S^S ligand do not affect the emission wavelength or color. However, they have a relatively considerable influence on the luminescence quantum yield values for which the complexes bearing cyclohexyl exhibit quantum yield values higher than those containing *n*-butyl (**1a** > **2a**). It arises from the higher structural rigidity of cyclohexyl in relation to that of *n*-butyl which results in the higher quantum yield.

The complexes with ppy ligand (**1a** and **2a**) include a peak at 490 nm with a vibronic progression at 520 nm (maximum) and a shoulder almost at 555 nm. Because of extending π-conjugation system, bzq complexes **1b** and **2b** are slightly red-shifted in relation to ppy complexes, in good agreement with the UV–vis spectra.[44] They exhibit relatively structured emission bands at 510 and 504 nm (for **1b** and **2b** respectively) with both vibronic progressions at 530 nm and shoulders at 570–580 nm region. The observed structured emission bands in the complexes indicate the superiority of the ligand-centered transitions (^{3}LC) rather than other available transitions with lower contribution of ^{3}MLCT transition.[44,45]

Upon cooling to 77 K, complexes become clearly structured and better emitters, exhibiting higher quantum yields, due to the imposition of extra rigidity. The low temperature bands all have blue-shifted compared with those of 298 K; therefore, no change in emission color is observed. This blueshift could be related to the improved rigidity in the freezing state, which has frequently defined as rigidochromism.[44,46] As mentioned above, complexes display a very strong luminescence in their frozen glassy states for which the corresponding emission bands almost match up with those observed for the solid state at 77 K showing the same types of transitions. However, the highest energy bands for bzq complexes **1b** and **2b** are intensified in comparison to their bands in solid state at 77 K, whereas those of ppy complexes remain almost unchanged.

DFT Calculations. The structure of **2b** was typically optimized in CH_2Cl_2 solution and solid state, including singlet (S_0) and triplet (T_1) states, by DFT calculations (see Figure 5 for the optimized structure of **2b** in CH_2Cl_2 solution and Table S1 for the geometrical parameters for all states). The crystal structure of this complex was used as the input file for the software. Besides, for **2b**, the energy levels of the important frontier molecular orbitals with their compositions were obtained for singlet and triplet states. Figure 6 represents the important MO plots of **2b** while the corresponding compositions are listed in Table 3.

For **2b** the HOMO–LUMO energy gap is found to be 3.766 eV. In HOMO, the maximum contribution coefficient belongs to d_{yz} and d_{xy} atomic orbitals of Pt1 center, while the p_y atomic orbitals of S1 and carbons and nitrogen of bzq ligand occupy the lower ranks. HOMO−1 almost resembles HOMO with the effective contribution of p_y of S2 atom whereas the HOMO−2 energy level is almost completely located on Pt1 atom. LUMO and LUMO+1 are predominantly localized on the p_y atomic orbitals of carbons and nitrogen of aromatic rings in bzq ligand; however, the major contribution of d_{xy} of Pt1 in LUMO+2 is followed by the considerable presence of s, p_x, and p_z atomic orbitals of the S1 and S2 atoms of btp ligand.

DOI: 10.1021/acs.organomet.7b00054
Organometallics XXXX, XXX, XXX–XXX

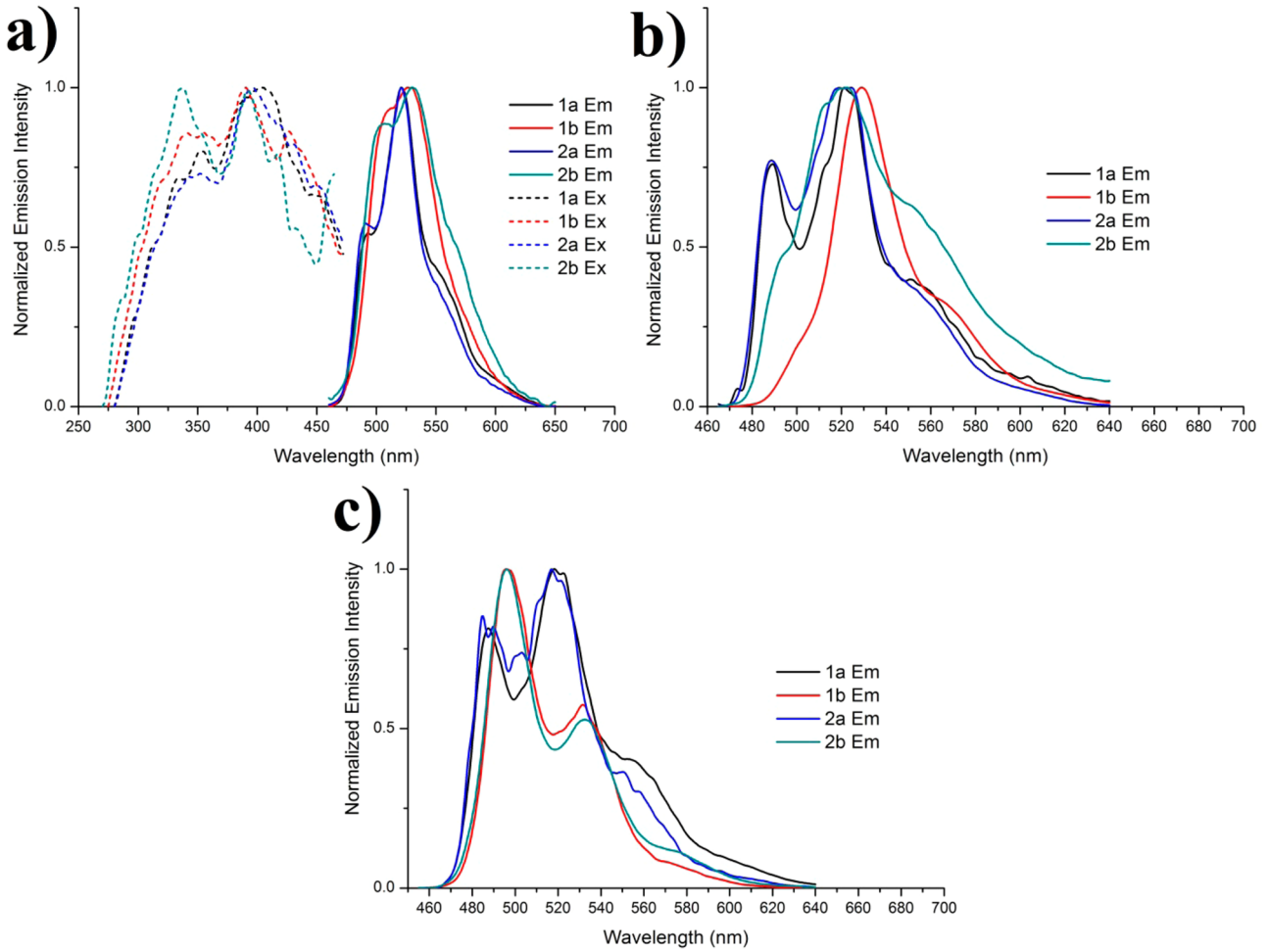

Figure 4. Normalized emission (solid lines) and excitation spectra (dashed lines) for **1** and **2** in (a) solid state at 298 K, (b) solid state at 77 K, and (c) CH_2Cl_2 glassy state.

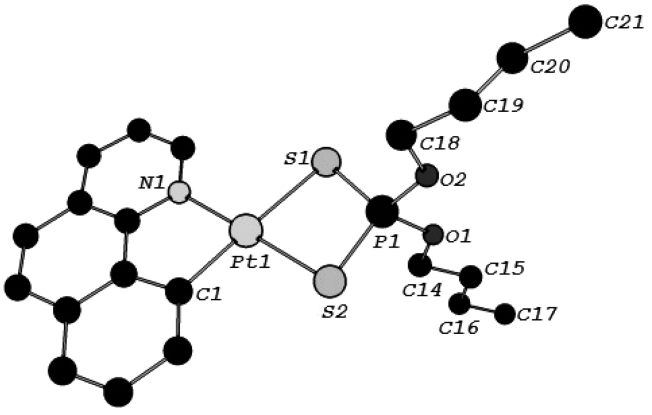

Figure 5. View of the DFT optimized structure of **2b** with the atom numbering. Hydrogen atoms are omitted for clarity.

In order to have a better picture for the available transitions in **2b**, TD-DFT calculations were employed using the optimized structure of this complex in CH_2Cl_2 solution. Figure 7 depicts the overlaid experimental absorbance spectrum and calculated TD-DFT bars for **2b**, of which an acceptable matching is observed between the experimental spectrum and calculated bars. Also, Table 4 summarizes the calculated transitions with their assignments. As can be seen in Figure 7, the absorptions around 405 nm include HOMO → LUMO and HOMO−1 → LUMO transitions that can be assigned as ^{1}ILCT transitions with some mixing of ^{1}MLCT and ^{1}L′LCT characters. At 353 nm, ^{1}L′LCT transition dominates, but the ILCT and MLCT transitions are still present. At higher energies, the role of btp ligand becomes more important; however, the ILCT predominates over the other transitions. The greatest contribution for the bands around 292 nm is related to the HOMO−4 → LUMO transition which has a mixed ^{1}ILCT/^{1}MLCT/^{1}L′LCT character. The main transitions for 256 nm are similar to those observed for previous ones; however, the intra btp ligand transitions are also observed at this wavelength.

The calculated emission of **2b** was also obtained by the optimization of the geometry of the lowest-energy triplet state T_1 in solid state. The theoretical phosphorescence wavelength, as the energy gap between the lowest optimized T_1 and S_0 in solid state, was calculated and found to be 475 nm for **2b**, which is qualitatively close to that of experimental spectrum with a relatively slight blue shift.

Biological Activity Studies. The *in vitro* cytotoxicity effects of **1** and **2** were evaluated against a panel of three cancer cell lines (lung carcinoma (A549), ovarian carcinoma (SKOV3), and breast carcinoma (MCF-7)). The most active complex of the series, **2a**, exhibited higher antiproliferative activity than *cis*-platin against SKOV3 and MCF-7 cells lines (Figures S17−S20 and Table 5). It displayed a strong

DOI: 10.1021/acs.organomet.7b00054
Organometallics XXXX, XXX, XXX−XXX

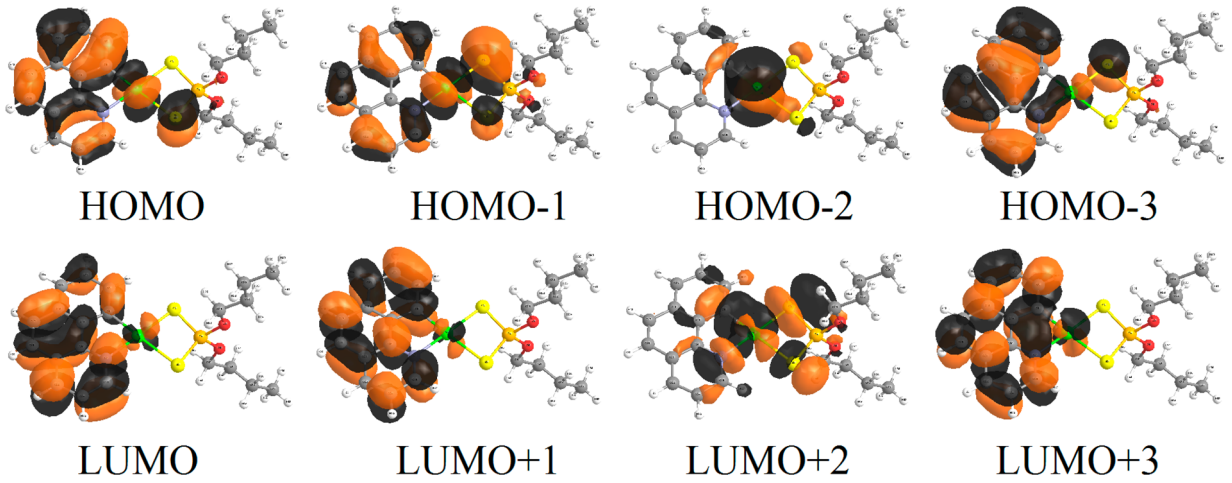

Figure 6. Important MO plot for **2b**.

Table 3. Energies of the Selected MOs of 2b and Their Compositions

		components (%)		
MO	energy (eV)	bzq	Pt	btp
LUMO+5	+0.386	23	28	49
LUMO+4	−0.229	2	3	95
LUMO+3	−0.335	93	5	2
LUMO+2	−0.910	25	38	37
LUMO+1	−1.316	95	4	1
LUMO	−1.931	95	4	1
HOMO	−5.697	48	40	12
HOMO−1	−6.037	17	46	37
HOMO−2	−6.286	7	89	4
HOMO−3	−6.639	78	11	12
HOMO−4	−6.726	34	29	37
HOMO−5	−7.080	38	10	52

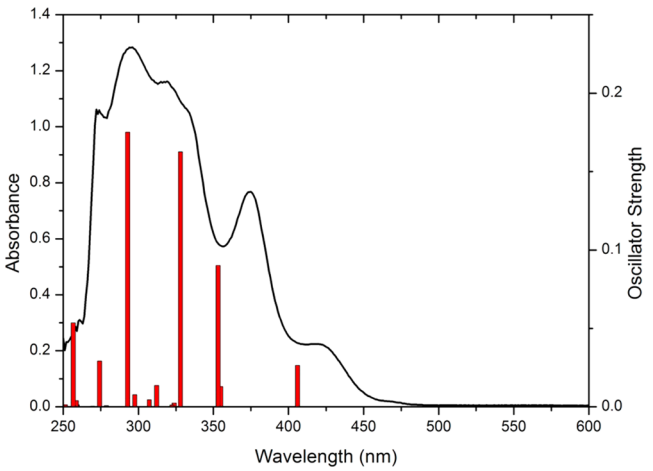

Figure 7. Overlaid experimental absorbance spectrum and calculated TD-DFT bars for **2b**.

antitumor activities with IC_{50}'s of 8.49 and 8.38 μM, compared with that measured for *cis*-platin which were 13.94 and 13.17 μM against SKOV3 and MCF-7 cell lines, respectively. It had also a moderate antitumor effect against A549 cell line activity with an IC_{50} of 12.35 μM. Among the three investigated complexes, **1b** revealed weak cytotoxicity against the studied cancer cells lines. **2b** presented higher antiproliferative activity than did **1a** against A549 and MCF-7 cancer cells lines. In contrast, **1a** showed a higher cytotoxic effect on SKOV3 cells line than did **2b**.

In general, it can be inferred that the presence of btp ligand (in **2a** and **2b**) has higher cytotoxicity activity than that of ctp ligand. Part of these data can be obtained from their interaction with DNA as their target. For example, molecular modeling studies revealed that **2b** has the best docking binding energies with DNA. This compound may exert its cytotoxic effect through different mechanism from *cis*-platin. We currently continue our study on these compounds to reveal its DNA binding activity (experimentally), effect on cell cycle, and other biological pathways.

DNA groove binding (in the major or minor groove of the DNA) and DNA intercalation are two of the most commonly observed modes of interaction of platinum anticancer agents with the DNA. In groove binding mode, the ligand is typically flexible, comprises rotatable bonds, and has the capability to orient itself along the major or minor groove of the DNA, as a result inhibiting regular function of DNA. However, DNA intercalators are typically inflexible planar molecules that stack in-between the DNA base pairs causing an intercalation gap to appear in the DNA helical structure.[47,48] As it was shown in Figure 8, the docked model suggests that the most favorable energetically conformation of the docked pose of **2b** interacts with the minor groove of 1BNA. The bzq group of **2b** fits into the minor groove of the DNA, and the btp group placed away from the gap. It interacts via its sulfur groups with C11, A5, and G4 base pairs and via the butyl moiety with C3 and G10 base pairs in the minor groove of DNA.

Fluorescence Microscopy Cellular Localization. Fluorescence emission properties of **1a** and **2a** were assessed using fluorescent microscopy imaging. For this purpose, the MCF-7 cells were incubated with two concentrations of these compounds: 40 μM for 30 min and IC_{50} concentration (75 and 10 μM for **1a** and **2a**, respectively), alone (as control) and in combination with propidium iodide (PI) as a DNA binding agent. Live and fixed cells were examined with a fluorescence microscope with different emission filters. According to our observation, both compounds show green light emission. As shown in Figure 9, both **1a** and **2a** penetrated into the cells and dispersed in the cytoplasm of the MCF-7 cells; however, we could not find any evidence of their presence in the nucleus (Figure 9, unfixed cells). We repeated the experiment again to

DOI: 10.1021/acs.organomet.7b00054
Organometallics XXXX, XXX, XXX−XXX

Table 4. Wavelengths and Corresponding Nature of Transitions for 2b[a]

calculated λ (nm) (f)	transitions (contribution)	assignment
405 (0.026)	HOMO → LUMO (0.68)	ILCT/MLCT/L′LCT
	HOMO−1 → LUMO (0.14)	L′LCT/ILCT/MLCT
	HOMO−1 → LUMO (0.59)	L′LCT/ILCT/MLCT
353 (0.090)	HOMO → LUMO+1 (0.21)	ILCT/MLCT/L′LCT
	HOMO−1 → LUMO (0.25)	L′LCT/ILCT/MLCT
	HOMO−3 → LUMO (0.17)	ILCT/L′LCT
	HOMO−4 → LUMO (0.48)	ILCT/MLCT/L′LCT
292 (0.175)	HOMO−1 → LUMO+1 (0.32)	L′LCT/MLCT/ILCT
	HOMO−3 → LUMO (0.30)	ILCT/L′LCT
	HOMO−4 → LUMO+1 (0.65)	ILCT/MLCT/L′LCT
256 (0.053)	HOMO → LUMO+4 (0.12)	ILCT/MLCT/L′LCT
	HOMO−5 → LUMO+2 (0.11)	IL′CT/L′MCT/MLCT

[a]Where M = Pt center, L = bzq, and L′ = btp ligands.

Table 5. *In Vitro* Cytotoxicity against Cancer Cell Lines

	IC_{50} (μM ± SEM)		
complex	A549	SKOV3	MCF-7
1a	69.58 ± 2.47	46.38 ± 2.69	74.67 ± 1.74
1b	>100	>100	>100
2a	12.35 ± 1.26	8.49 ± 1.37	8.38 ± 1.83
2b	45.48 ± 2.48	48.29 ± 2.17	62.27 ± 3.38
cis-platin	1.63 ± 0.49	13.94 ± 1.61	13.17 ± 2.06

provide enough time for our compounds to diffuse through the cells, 48 h. As evident in Figure 9, the same pattern of cell staining could be also observed after a long incubation time, though both complexes show brighter cell staining than at 30 min staining time which could be due to increasing in their differential fluorescence emission as result of their interactions with a particular molecular microenvironment in the cell. In addition, our results indicated that contrary to **1a** which more homogeneously stains cytoplasm (in fixed cells) or localizes in some special intracellular compartments (white arrows in unfixed cells, Figure 9) **2a** preferably localizes in the cytoplasm in the perinuclear area. Perinuclear cytoplasm as well as nuclear localization of some platinum(II) complexes was also observed by Berenguer et al.[49] They show that these complexes, similar to our compounds, could be seen in the cytoplasm, especially in perinuclear region and/or penetrate into the nucleus.

CONCLUSION

Herein, a series of closely related heteroleptic cycloplatinated-(II) complexes have been prepared featuring *O*,*O*′-di(alkyl)-dithiophosphate as a bidentate anionic ancillary ligand (S^S). The new complexes exhibit strong green emissions at room temperature because of high intrinsic rigidity imposed by C^N and S^S chelates. Also, both bite angles of the chelates are considerably smaller than 90°, indicating the chelates are under strain and the molecule cannot undergo the molecular motions. For these ancillary ligands, it was found that the nature of R groups does not have any influence on the absorbance or emission of the molecules. Conversely, the C^N cyclomtalated ligand has a determining role in the emission properties of the

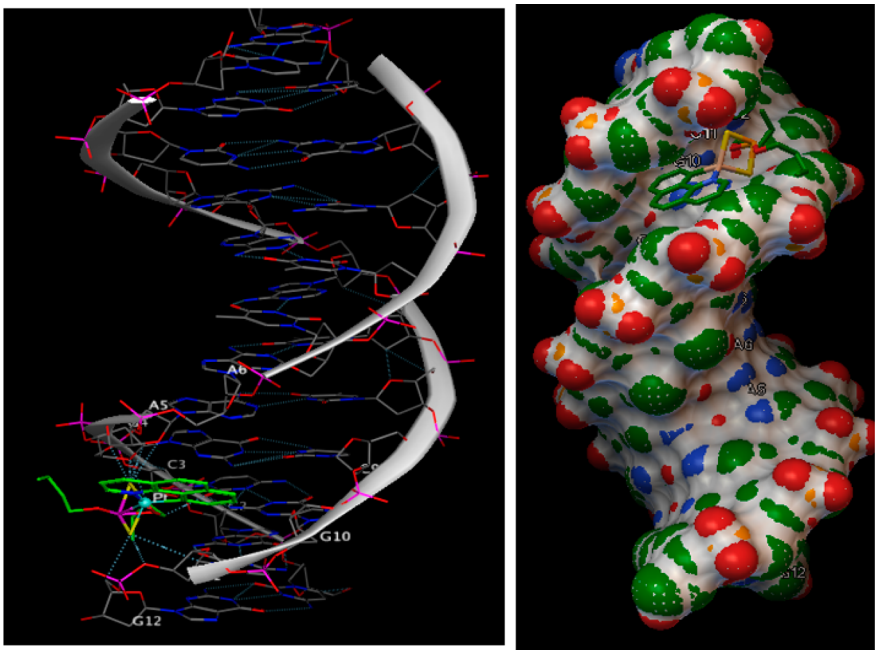

Figure 8. Molecular docking simulation studies of the interaction between **2b** and DNA (PDB ID: 1BNA).

DOI: 10.1021/acs.organomet.7b00054
Organometallics XXXX, XXX, XXX−XXX

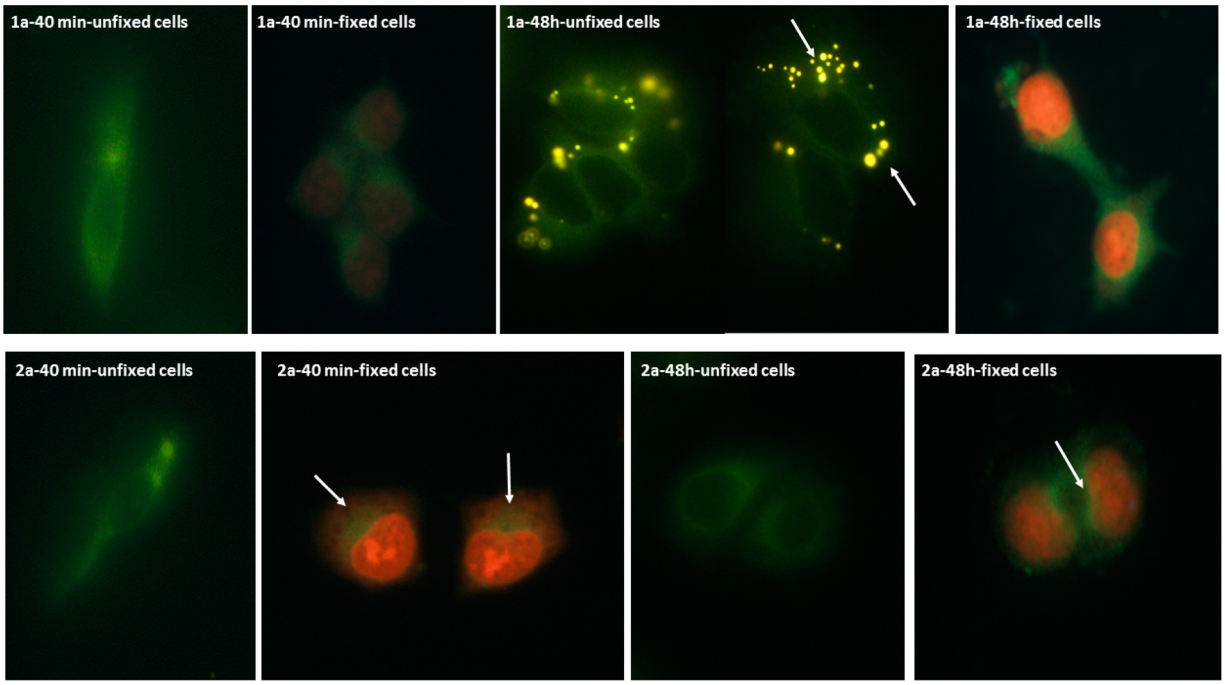

Figure 9. Intracellular tracking of compounds **1a** and **2a** in MCF-7 cells. MCF-7 cells were treated with **1a** and **2a** at 2 concentrations and 2 time points (labeled appropriately) and investigated immediately by a fluorescent microscope with or without fixation in the presence of propidium iodide (PI) as a DNA staining agent. **1a** (top) stains the cells' cytoplasm more homogeneously in the fixed cells (green color) or localized in special compartment in the cytoplasm (shiny spots, white arrows in unfixed cells), while **2a** (bottom) preferably localizes in perinuclear areas (white arrows).

molecules. As expected, the complexes possessing bzq ligand (**1b** and **2b**) have a redshift with respect to their ppy analogous (**1a** and **2a**) in both absorbance and emission spectra which is due to extending the π-conjugation system in bzq in comparison to ppy.[44]

The emission band shape and wavelength do not depend on the excitation wavelength over the wide range of 340−500 nm for excitation. The appearance of structured emission bands is indicative of the presence of a large amount of ^{3}LC (ligand centered) with a lower contribution of ^{3}MLCT transition in the emissive states. This is confirmed by the TD-DFT calculations which demonstrate that the transitions in the cyclometalated moieties are the predominant electronic transitions in the region between 295 and 500 nm; this region was employed for excitation wavelength to yield emission bands. Furthermore, at low temperatures (77 K), these bands become more intense and more structured without any considerable change in the wavelength. There is no any aggregation or excimeric interactions in the emission bands of complexes.

The cytotoxic activities of **1** and **2** were evaluated against different cancerous cell lines. The results illustrated that **2a** has satisfactory cytotoxic activity and the highest potency, while other complexes exhibited less cytotoxic activity. **2a** displayed significantly higher *in vitro* cytotoxicity than that of *cis*-platin against SKOV3 and MCF-7 cells lines. Fluorescence microscopy presented effective localization of **1a** and **2a** on MCF-7 human cells.

EXPERIMENTAL SECTION

General Procedures and Materials. All the reactions were carried out in common solvents, and all solvents were purified and dried according to standard procedures. The microanalyses were performed using a vario EL CHNS elemental analyzer and also all the melting point values were measured by a Buchi 510. Electrospray ion mass spectrum (ESI-MS) was recorded by a HP-5989B spectrometer using methanol−water as the mobile phase. Fourier transform infrared spectroscopy on KBr pellets was performed on a FT IR Bruker Vector 22 instrument. Multinuclear (^{1}H,^{13}C and ^{31}P) NMR spectra were recorded on a Bruker Avance DPX 400 MHz spectrometer at 298 K. All chemical shifts are reported in ppm (part per million) relative to their corresponding external standards ($SiMe_4$ for ^{1}H,^{13}C and 85% H_3PO_4 for ^{31}P{H}), and all the coupling constants (J values) are given in Hz. UV−vis spectra were recorded using a PerkinElmer Lambda 25 spectrophotometer. Photoluminescence spectra were recorded on a PerkinElmer LS45 fluorescence spectrometer at room and low temperatures, and the lifetimes were measured in phosphorimeter mode. The quantum yields of the complexes were measured using an integrating sphere. Also, the quantum yields at 77 K were obtained by indirect method based on the intensity change versus temperature by calculation concerning relative peak area changes in comparison with corresponding peak at ambient temperature. Complexes [Pt(C^N)(Cl)(dmso)], C^N = ppy[34] and bzq,[35] were prepared as reported in literature. The NMR labeling for the ligands are shown in Scheme 4 for clarifying the chemical shift assignments.

Potassium *O*,*O*′-di(cyclohexyl)dithiophosphate (**Kctp**) and potassium *O*,*O*′-di(butyl)dithiophosphate (**Kbtp**) were prepared in quantitative yield by published method with slight modification.[50−54]

Scheme 4. Representative Ligands with Position Labeling

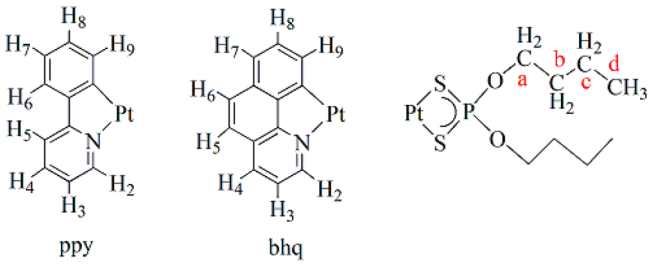

DOI: 10.1021/acs.organomet.7b00054
Organometallics XXXX, XXX, XXX−XXX

Potassium carbonate (10 mmol, 1.38 g) was added to a mixture of phosphorus pentasulfide (2.5 mmol, 1.11 g) in desired alcohol (5 mL, excess) at 60 °C. The reaction mixture was stirred for 2 h at 80 °C. The reaction mixture was filtered while hot to remove unreacted potassium carbonate. The filtrate was allowed to cool, and pure potassium *O,O′*-di(alkyl)dithiophosphate was crystallized in quantitative yield as a white solid that could be recrystallized in ethanol.

*Potassium O,O′-Di(butyl)dithiophosphate (**Kbtp**).* White solid; mp: 147−149 °C. NMR data in D_2O: $\delta(^1H)$ 0.81 (6H, t, J = 7.2 Hz), 1.28 (4H, sxt, J = 8.0 Hz), 1.53 (4H, qui, J = 6.8 Hz), 3.80−3.90 (4H, m); $\delta(^{13}C)$ 13.0, 18.4, 31.5 (d, J_{CP} = 9 Hz), 66.6 (d, J_{CP} = 8 Hz); $\delta(^{31}P)$ 111.2.

*Potassium O,O′-Di(cyclohexyl)dithiophosphate (**Kctp**).* White solid; mp: 262−264 °C. NMR data in D_2O: $\delta(^1H)$ 1.09−1.28 (6H, m), 1.32−1.45 (6H, m), 1.61−1.65 (4H, m), 1.88−1.92 (4H, m), 4.26−4.37 (2H, m); $\delta(^{13}C)$ 23.7, 24.8, 33.3 (d, J_{CP} = 4 Hz), 77.4 (d, J_{CP} = 9 Hz); $\delta(^{31}P)$ 107.5.

*[Pt(ppy)(ctp)], **1a**.* A solution of **Kctp** (36 mg, 0.11 mmol) in ethanol (15 mL) was added to a solution of [Pt(ppy) (Cl) (dmso)] (50 mg, 0.11 mmol) in acetone (5 mL) under an Ar atmosphere. After stirring for 3 h at room temperature, a yellow solution was formed. Then, the solvent was evaporated, and the residue was treated with CH_2Cl_2. The obtained solution was filtered through Celite to remove KCl. After evaporation of the solvent under reduced pressure, the residue was washed with *n*-hexane (2 × 3 mL). The precipitate as a yellow solid was dried under vacuum. Yield: 61 mg, 86%; mp = 220 °C. MS ESI(+): m/z 643.11 $[M]^+$. Elem. Anal. Calcd for $C_{23}H_{30}NO_2PPtS_2$ (642.7): C, 42.98; H, 4.71; N, 2.18. Found: C, 43.13; H, 4.65; N, 2.21. IR: 683 cm^{-1} (P═S), 540 cm^{-1} (P−S). NMR data in $CDCl_3$: $\delta(^1H)$ 1.26−1.74 (m, 16H, overlapping multiplets of cyclohexyl groups), 2.03−2.06 (m, 4H, overlapping multiplets of cyclohexyl groups), 4.61−4.68 (m, 2H, CH of cyclohexyl groups adjacent to O atom), 7.07 (t, $^3J_{HH}$ = 6.1 Hz, 1H, H^8), 7.11−7.19 (m, 2H, H^7 and H^3), 7.44 (d, $^3J_{HH}$ = 5.7 Hz, $^3J_{PtH}$ = 56.4 Hz, 1H, H^9), 7.53 (m, 1H, H^6), 7.74 (d, $^3J_{HH}$ = 7.8 Hz, 1H, H^5) 7.86 (t, $^3J_{HH}$= 7.7 Hz, 1H, H^4), 8.78 (d, $^3J_{HH}$ = 5.5 Hz, $^3J_{PtH}$ = 43.1 Hz, 1H, H^2); $\delta(^{31}P)$ 96.8 (s, $^2J_{PH}$ = 323 Hz, 1P of ctp). The other complexes were made similarly using the appropriate precursor complexes and ligands.

*[Pt(bzq)(ctp)], **1b**.* Yield: 57 mg, 73%; mp = 246 °C. MS ESI(+): m/z 667.11 $[M]^+$. Elem. Anal. Calcd for $C_{25}H_{30}NO_2PPtS_2$ (666.7): C, 45.04; H, 4.54; N, 2.10. Found: C, 45.11; H, 4.48; N, 2.14. IR: 707 cm^{-1} (P═S), 506 cm^{-1} (P−S). NMR data in $CDCl_3$: $\delta(^1H)$ 1.21−1.77 (m, 16H, overlapping multiplets of cyclohexyl groups), 2.05−2.09 (m, 4H, overlapping multiplets of cyclohexyl groups), 4.65−4.74 (m, 2H, CH of cyclohexyl groups adjacent to O atom), 7.44 (dd, $^3J_{HH}$ = 7.9 Hz, $^4J_{PH}$ = 5.4 Hz, 1H, H^8), 7.53 (t, $^3J_{HH}$ = 7.5 Hz, 1H, H^3), 7.57 (d, $^3J_{HH}$ = 8.7 Hz, 1H, H^6), 7.66 (d, $^3J_{HH}$ = 8.1 Hz, $^3J_{PtH}$ = not resolved Hz, 1H, H^9), 7.69 (m, 1H, H^7), 7.79 (d, $^3J_{HH}$ = 8.7 Hz, 1H, H^5), 8.36 (dd, $^3J_{HH}$ = 8.1 Hz, $^4J_{HH}$ = 1.2 Hz, 1H, H^4), 9.02 (dd, $^3J_{HH}$ = 5.4 Hz, $^4J_{HH}$ = 1.2 Hz, $^3J_{PtH}$ = 43.8 Hz, 1H, H^2); $\delta(^{31}P)$ 98.2 (s, $^2J_{PH}$ = 343 Hz, 1P of ctp).

*[Pt(ppy)(btp)], **2a**.* Yield: 53 mg, 82%; mp = 226 °C. MS ESI(+): m/z 591.08 $[M]^+$. Elem. Anal. Calcd for $C_{19}H_{26}NO_2PPtS_2$ (590.6): C, 38.64; H, 4.44; N, 2.37. Found: C, 38.77; H, 4.51; N, 2.28. IR: 737 cm^{-1} (P═S), 516 cm^{-1} (P−S). NMR data in $CDCl_3$: $\delta(^1H)$ 0.94 (t, $^3J_{HH}$ = 7.4 Hz, 6H, H^d), 1.38−1.49 (m, 4H, H^c), 1.71−1.78 (m, 4H, H^b), 4.21 and 4.23 (t, $^3J_{HH}$ = 6.6 and 6.6 Hz, 4H, H^a), 7.09 (td, $^3J_{HH}$ = 6.5 Hz,$^4J_{HH}$ = 1.2 Hz, 1H, H^8), 7.12−7.17 (m, 2H, H^7 and H^3), 7.44 (m, $^3J_{PtH}$ = not resolved, 1H, H^9), 7.53 (dd,$^3J_{HH}$ = 5.8 Hz, $^4J_{HH}$ = 3.4 Hz, 1H, H^6), 7.74 (d, $^3J_{HH}$ = 7.8 Hz, 1H, H^5), 7.87 (td, $^3J_{HH}$ = 7.7 Hz, $^4J_{HH}$ = 1.5 Hz, 1H, H^4), 8.79 (d, $^3J_{HH}$ = 5.7 Hz, $^3J_{PtH}$ = 43.4 Hz, 1H, H^2); $\delta(^{31}P)$ 100.8 (s, $^2J_{PH}$ = 320 Hz, 1P of btp).

*[Pt(bzq)(btp)], **2b**.* Yield: 59 mg, 87%; mp = 238 °C. MS ESI(+): m/z 615.08 $[M]^+$. Elem. Anal. Calcd for $C_{21}H_{26}NO_2PPtS_2$ (614.6): C, 41.04; H, 4.26; N, 2.28. Found: C, 41.13; H, 4.21; N, 2.35. IR: 711 cm^{-1} (P═S), 459 cm^{-1} (P−S). NMR data in $CDCl_3$: $\delta(^1H)$ 0.95 (t, $^3J_{HH}$ = 7.4 Hz, 6H, H^d), 1.41−150 (m, 4H, H^c), 1.73−1.80 (m, 4H, H^b), 4.25 and 4.27 (t, $^3J_{HH}$ = 6.6 and 6.6 Hz, 4H, H^a), 7.44 (dd, $^3J_{HH}$ = 8.1 Hz, $^4J_{PH}$ = 5.34 Hz, 1H, H^8), 7.53 (t, $^3J_{HH}$ = 7.7 Hz, 1H, H^3), 7.57 (d, $^3J_{HH}$ = 8.8 Hz, 1H, H^6), 7.59−7.76 (m, 2H, H^9 and H^7), 7.79 (d, $^3J_{HH}$ = 8.7 Hz, 1H, H^5), 8.36 (dd, $^3J_{HH}$ = 8.1 Hz, $^4J_{HH}$ = 0.9 Hz, 1H, H^4), 9.02 (dd, $^3J_{HH}$ = 5.4 Hz, $^4J_{HH}$ = 0.9 Hz, $^3J_{PtH}$ = 44.2 Hz, 1H, H^2); $\delta(^{31}P)$ 102.1 (s, $^2J_{PH}$ = 341.9 Hz, 1P of btp).

Computational Details. The geometries of complexes were fully optimized by employing the density functional theory without imposing any symmetry constraints. Density functional calculations were performed with the program suite Gaussian03[55] using the B3LYP level of theory.[56−58] The effective core potential of Hay and Wadt basis set (LANL2DZ) basis set was chosen to describe Pt and I atoms.[59,60] The 6-31G(d) basis set was used for the other atoms.

X-ray Structure Determinations. The X-ray diffraction measurements were carried out on STOE IPDS-2/2T diffractometer with graphite-monochromated Mo Kα radiation. All single crystals were mounted on a glass fiber and used for data collection. Cell constants and an orientation matrix for data collection were obtained by least-squares refinement of the diffraction data. Diffraction data were collected in a series of ω scans in 1° oscillations and integrated using the Stoe X-AREA[61] software package. A numerical absorption correction was applied using X-RED[62] and X-SHAAPE[63] software. The data were corrected for Lorentz and polarizing effects. The structures were solved by direct methods[64] and subsequent difference Fourier maps and then refined on F^2 by a full-matrix least-squares procedure using anisotropic displacement parameters.[65] Atomic factors are from *International Tables for X-ray Crystallography*.[66] All non-hydrogen atoms were refined with anisotropic displacement parameters. Hydrogen atoms were placed in ideal positions and refined as riding atoms with relative isotropic displacement parameters. All refinements were performed using the X-STEP32 crystallographic software package.[67] Crystallographic and structure refinement data are collected in Table S2.

Biological Assay. *Cell Lines and Cell Culture.* Human cancer cell lines, A549 (nonsmall cell lung cancer), SKOV3 (ovarian cancer), and MCF-7 (breast cancer), were obtained from National Cell Bank of Iran (NCBI, Pasteur Institute, Tehran, Iran). All cells were cultured in DMEM medium (Biosera, UK), except MCF-7 cells which were cultured in RPMI 1640, supplemented with 10% fetal bovine serum (FBS; Gibco, USA) and pencilin−streptomycin and were incubated at 37 °C in humidified CO_2 incubator.

Cytotoxic activities of **1** and **2** were assessed by using a standard 3-(4,5-dimethylthiazol-yl)-2,5-diphenyl-tetrazolium bromide (MTT) assay. Briefly, the assay was performed according to a known protocol.[47,48,68] The cells were harvested and plated in 96-well microplates at a density of 1×10^4 cells per well in 180 μL of complete culture media. After 24 h of incubation, each cell was treated with five different concentrations of the compounds ranging from 1×10^{-4} to 1×10^{-7} M. Each compound was dissolved in DMSO, and the final concentration of DMSO was maintained at about 0.1% to avoid its bystander cytotoxic effect. After 48 h of incubation at 37 °C in humidified CO_2 incubator, media were completely removed and replaced with 150 μL of media containing 0.5 mg/mL MTT solution and the plate were incubated for 3 h at room temperature. The media containing MTT was then discarded, and 150 μL of DMSO was added to each well to dissolve the formazan crystals. The solutions were incubated overnight. The absorbance in individual wells was obtained at 570 nm using Bio-Rad microplate reader (Model 680). Data was analyzed and expressed as the 50% inhibitory concentrations (IC_{50}), which were tested four times for each complex in triplicate manner. Data are presented as mean ± SEM.

Molecular Docking. The docking simulations were carried out by means of AutoDock 4.2.[69] The three-dimensional crystal structures of DNA (Protein Databank ID: 1BNA) were retrieved from Protein Databank (www.rcsb.org/pdb). All water molecules were removed, missing hydrogens were added, and the Kollman united atom charges were determined. Subsequently, the PDB were converted to PDBQT using MGLTOOLS 1.5.6. In all experiments, Lamarchian genetic algoritm search method was used to find the best pose of each ligand in the active site of the DNA. The grid center on the DNA structures was maintained by centering the grid box on the minor groove, major groove, and the intercalation site to cover the full of DNA structure.

DOI: 10.1021/acs.organomet.7b00054
Organometallics XXXX, XXX, XXX−XXX

The grid maps had a spacing of 0.375 Å. All the other parameters were kept at their default values. Parameters for docking with metal ions such as platinum, used in the docking calculation, were added to gpf and dpf files.

The structure of **2b** was created by HyperChem Professional (Version 8, Hypercube Inc., Gainesville, FL). **2b** was optimized by molecular mechanic methods (MM^+) using HyperChem 8, followed by energy minimization calculations at Hartree−Fock (HF) level using Gaussian 09. The output structure was thereafter converted to PDBQT using MGLtools 1.5.6. All calculations were run on a core i7 personal computer (CPU at 8 MB) with Windows 7 operating system. With respect to the AutoDock scoring function, the lowest docking binding energy conformation was chosen as the best binding mode. Visualization of the docked pose has been performed by means of AutoDock Tools 1.5.6 and PyMOL molecular graphics program.[70] Crystallographic data (excluding structure factors) for the structural analysis has been deposited with the Cambridge Crystallographic Data Centre under Accession No. 1527164.

Localization in Cells. As mentioned, our compounds showed fluorescence emission properties, and we used this to track two of our effective compounds (**1a** and **2a**) in the host cells. To do this, MCF7 cells were cultured over coverslips into a 6-well plate with 2 mL of complete culture media per well for 24 h. The cells were then separated into two groups: The first was incubated with 2 mL of new medium containing 40 μM each compound (**1a** and **2a**) at 37 °C for 30 min. The cells in second group, based on their IC_{50}, were incubated with 75 and 10 μM **1a** and **2a**, respectively, for 48 h at 37 °C. After incubation, the cells were washed twice in 1× phosphate-buffered saline (PBS, pH 7.2) and fixed with cold absolute methanol for 10 min (Merck, Germany). The cells were then washed with PBS, dried at room temperature, and stained with 0.25 μg/mL PI (BD Biosciences, USA) prepared in glycerol. PI is a fluorescent molecule that intercalates with DNA and can be used to stain cell nuclei. To control the light emission interference between channels and to check the presence of drugs in the nucleus, the cells were also incubated separately with each compound and were visualized without fixation and PI staining. The cells were finally washed twice with 1× PBS (pH 7.2). Coverslips were then removed, mounted on glass slides with glycerol, and immediately examined under a fluorescence microscope (BX61, Olympus, Japan). The images were taken at 100× magnification and analyzed by the Olympus micro imaging software cellSens (Olympus, Japan).

■ ASSOCIATED CONTENT

Supporting Information

The Supporting Information is available free of charge on the ACS Publications website at DOI: 10.1021/acs.organomet.7b00054.

NMR spectra, crystallographic and computational details (PDF)
Crystallographic data (CIF)
Optimized geometries (XYZ)

■ AUTHOR INFORMATION

Corresponding Author

*Phone: (+98) 24 3315 3206. E-mail: shahsavari@iasbs.ac.ir.

ORCID

Hamid R. Shahsavari: 0000-0002-2579-2185

Notes

The authors declare no competing financial interest.

■ ACKNOWLEDGMENTS

This work was supported by the Institute for Advanced Studies in Basic Sciences (IASBS) Research Council and the Iran National Science Foundation (grant no. 95822524 and 95834232). The collaboration of Medicinal Chemistry, Faculty of Pharmacy, Ahvaz Jundishapur University of Medical Sciences, in providing the required facilities for this work is greatly acknowledged. The technical support of the Chemistry Computational Center at Shahid Beheshti University is gratefully acknowledged. This paper is extracted from Ms. Tabassom Mirzaee's thesis (B-94/061). Thanks are also due to Mr. A. Biglari, the operator of Bruker NMR instrument at IASBS, for recording the NMR spectra and Prof. M. T. Moreno, Universidad de La Rioja, for ESI-MS measurements. This paper is dedicated to the memory of Professor Mehdi Rashidi who recently passed away. He was the founder of organometallic field in Iran.

■ REFERENCES

(1) Berenguer, J. R.; Lalinde, E.; Martín, A.; Moreno, M. T.; Sánchez, S.; Shahsavari, H. R. *Inorg. Chem.* **2016**, *55*, 7866−7878.
(2) Micksch, M.; Tenne, M.; Strassner, T. *Organometallics* **2014**, *33*, 3464−3473.
(3) Tarran, W. A.; Freeman, G. R.; Murphy, L.; Benham, A. M.; Kataky, R.; Williams, J. G. *Inorg. Chem.* **2014**, *53*, 5738−5749.
(4) Moussa, J.; Cheminel, T.; Freeman, G. R.; Chamoreau, L.-M.; Williams, J. G.; Amouri, H. *Dalton Trans.* **2014**, *43*, 8162−8165.
(5) Hofbeck, T.; Lam, Y. C.; Kalbáč, M.; Záliš, S.; Vlček, A., Jr; Yersin, H. *Inorg. Chem.* **2016**, *55*, 2441−2449.
(6) Bossi, A.; Rausch, A. F.; Leitl, M. J.; Czerwieniec, R.; Whited, M. T.; Djurovich, P. I.; Yersin, H.; Thompson, M. E. *Inorg. Chem.* **2013**, *52*, 12403−12415.
(7) Chan, M. H.-Y.; Wong, H.-L.; Yam, V. W.-W. *Inorg. Chem.* **2016**, *55*, 5570−5577.
(8) Chen, Y.; Lu, W.; Che, C.-M. *Organometallics* **2013**, *32*, 350−353.
(9) Lu, W.; Mi, B.-X.; Chan, M. C. W.; Hui, Z.; Zhu, N.; Lee, S.-T.; Che, C.-M. *Chem. Commun.* **2002**, 206−207.
(10) Lu, W.; Mi, B.-X.; Chan, M. C.; Hui, Z.; Che, C.-M.; Zhu, N.; Lee, S.-T. *J. Am. Chem. Soc.* **2004**, *126*, 4958−4971.
(11) Schneider, J.; Du, P.; Jarosz, P.; Lazarides, T.; Wang, X.; Brennessel, W. W.; Eisenberg, R. *Inorg. Chem.* **2009**, *48*, 4306−4316.
(12) Pashaei, B.; Shahroosvand, H.; Graetzel, M.; Nazeeruddin, M. K. *Chem. Rev.* **2016**, *116*, 9485−9564.
(13) Yam, V. W. W.; Tang, R. P. L.; Wong, K. M. C.; Lu, X. X.; Cheung, K. K.; Zhu, N. *Chem. - Eur. J.* **2002**, *8*, 4066−4076.
(14) Lanoë, P.-H.; Le Bozec, H.; Williams, J. G.; Fillaut, J.-L.; Guerchais, V. *Dalton Trans.* **2010**, *39*, 707−710.
(15) Siu, P. K.; Lai, S. W.; Lu, W.; Zhu, N.; Che, C. M. *Eur. J. Inorg. Chem.* **2003**, *2003*, 2749−2752.
(16) Strassner, T. *Acc. Chem. Res.* **2016**, *49*, 2680−2689.
(17) Williams, J. A. G. *Top. Curr. Chem.* **2007**, *281*, 205−268.
(18) Lamansky, S.; Djurovich, P. I.; Abdel-Razzaq, F.; Garon, S.; Murphy, D. L.; Thompson, M. E. *J. Appl. Phys.* **2002**, *92*, 1570−1575.
(19) Chen, L.; You, H.; Yang, C.; Zhang, X.; Qin, J.; Ma, D. *J. Mater. Chem.* **2006**, *16*, 3332−3339.
(20) Liu, Y.; Ye, K.; Fan, Y.; Song, W.; Wang, Y.; Hou, Z. *Chem. Commun.* **2009**, 3699−3701.
(21) Lee, T. C.; Chang, C. F.; Chiu, Y. C.; Chi, Y.; Chan, T. Y.; Cheng, Y. M.; Lai, C. H.; Chou, P. T.; Lee, G. H.; Chien, C. H.; et al. *Chem. - Asian J.* **2009**, *4*, 742−753.
(22) You, Y.; Seo, J.; Kim, S. H.; Kim, K. S.; Ahn, T. K.; Kim, D.; Park, S. Y. *Inorg. Chem.* **2008**, *47*, 1476−1487.
(23) Niedermair, F.; Waich, K.; Kappaun, S.; Mayr, T.; Trimmel, G.; Mereiter, K.; Slugovc, C. *Inorg. Chim. Acta* **2007**, *360*, 2767−2777.
(24) Ionkin, A. S.; Marshall, W. J.; Wang, Y. *Organometallics* **2005**, *24*, 619−627.
(25) Leopold, H.; Strassner, T. *Organometallics* **2016**, *35*, 4050−4059.
(26) Brooks, J.; Babayan, Y.; Lamansky, S.; Djurovich, P. I.; Tsyba, I.; Bau, R.; Thompson, M. E. *Inorg. Chem.* **2002**, *41*, 3055−3066.
(27) Moussa, J.; Chamoreau, L. M.; Gullo, M. P.; Degli Esposti, A.; Barbieri, A.; Amouri, H. *Dalton Trans.* **2016**, *45*, 2906−2913.

DOI: 10.1021/acs.organomet.7b00054
Organometallics XXXX, XXX, XXX−XXX

(28) Sesolis, H.; Moussa, J.; Gontard, G.; Jutand, A.; Gullo, M. P.; Barbieri, A.; Amouri, H. *Dalton Trans.* **2015**, *44*, 2973−2977.
(29) Forniés, J.; Sicilia, V.; Casas, J. M.; Martín, A.; López, J. A.; Larraz, C.; Borja, P.; Ovejero, C. *Dalton Trans.* **2011**, *40*, 2898−2912.
(30) Ghavale, N.; Wadawale, A.; Dey, S.; Jain, V. K. *J. Organomet. Chem.* **2010**, *695*, 1237−1245.
(31) Ghavale, N.; Wadawale, A.; Dey, S.; Jain, V. K. *J. Organomet. Chem.* **2010**, *695*, 2296−2304.
(32) Haiduc, I. 1,1-Dithiolato Ligands. In *Comprehensive Coordination Chemistry II*; Meyer, T. J., Ed.; Pergamon: Oxford, 2003; pp 349−376.
(33) Haiduc, I.; Sowerby, D. B.; Lu, S.-F. *Polyhedron* **1995**, *14*, 3389−3472.
(34) Pazderski, L.; Pawlak, T.; Sitkowski, J.; Kozerski, L.; Szłyk, E. *Magn. Reson. Chem.* **2009**, *47*, 932−941.
(35) Godbert, N.; Pugliese, T.; Aiello, I.; Bellusci, A.; Crispini, A.; Ghedini, M. *Eur. J. Inorg. Chem.* **2007**, *2007*, 5105−5111.
(36) Fackler, J. P.; Thompson, L. D.; Lin, I. J. B.; Stephenson, T. A.; Gould, R. O.; Alison, J. M. C.; Fraser, A. J. F. *Inorg. Chem.* **1982**, *21*, 2397−2403.
(37) Niazi, M.; Shahsavari, H. R.; Golbon Haghighi, M.; Halvagar, M. R.; Hatami, S.; Notash, B. *RSC Adv.* **2016**, *6*, 76463−76472.
(38) Niazi, M.; Shahsavari, H. R.; Golbon Haghighi, M.; Halvagar, M. R.; Hatami, S.; Notash, B. *RSC Adv.* **2016**, *6*, 95073−95084.
(39) Balashev, K. P.; Puzyk, M. V.; Kotlyar, V. S.; Kulikova, M. V. *Coord. Chem. Rev.* **1997**, *159*, 109−120.
(40) Díez, A.; Forniés, J.; García, A.; Lalinde, E.; Moreno, M. T. *Inorg. Chem.* **2005**, *44*, 2443−2453.
(41) DePriest, J.; Zheng, G. Y.; Goswami, N.; Eichhorn, D. M.; Woods, C.; Rillema, D. P. *Inorg. Chem.* **2000**, *39*, 1955−1963.
(42) Maestri, M.; Sandrini, D.; Balzani, V.; von Zelewsky, A.; Jolliet, P. *Helv. Chim. Acta* **1988**, *71*, 134−139.
(43) Chi, Y.; Chou, P.-T. *Chem. Soc. Rev.* **2010**, *39*, 638−655.
(44) Jamshidi, M.; Nabavizadeh, S. M.; Shahsavari, H. R.; Rashidi, M. *RSC Adv.* **2015**, *5*, 57581−57591.
(45) Berenguer, J. R.; Díez, Á.; Lalinde, E.; Moreno, M. T.; Ruiz, S.; Sánchez, S. *Organometallics* **2011**, *30*, 5776−5792.
(46) Chen, P.; Meyer, T. J. *Chem. Rev.* **1998**, *98*, 1439−1478.
(47) Fereidoonnezhad, M.; Niazi, M.; Ahmadipour, Z.; Mirzaee, T.; Faghih, Z.; Faghih, Z.; Shahsavari, H. R. *Eur. J. Inorg. Chem.* **2017**, 2247−2254.
(48) Fereidoonnezhad, M.; Niazi, M.; Shahmohammadi Beni, M.; Mohammadi, S.; Faghih, Z.; Faghih, Z.; Shahsavari, H. R. *ChemMedChem* **2017**, *12*, 456−465.
(49) Berenguer, J. R.; Pichel, J. G.; Gimenez, N.; Lalinde, E.; Moreno, M. T.; Pineiro-Hermida, S. *Dalton Trans.* **2015**, *44*, 18839−18855.
(50) Kaboudin, B.; Elhamifar, D. *Synthesis* **2006**, *2006*, 224−226.
(51) Kaboudin, B.; Malekzadeh, L. *Synlett* **2011**, *2011*, 2807−2810.
(52) Kaboudin, B.; Yarahmadi, V.; Kato, J.-y.; Yokomatsu, T. *RSC Adv.* **2013**, *3*, 6435−6441.
(53) Kaboudin, B.; Elhamifar, D.; Farjadian, F. *Org. Prep. Proced. Int.* **2006**, *38*, 412−417.
(54) Bond, A. M.; Colton, R.; Dakternieks, D.; Dillon, M. L.; Hauenstein, J.; Moir, J. E. *Aust. J. Chem.* **1981**, *34*, 1393−1400.
(55) Frisch, M. J.; Trucks, G. W.; Schlegel, H. B.; Scuseria, G. E.; Robb, M. A.; Cheeseman, J. R.; Montgomery, J. A., Jr.; Vreven, T.; Kudin, K. N.; Burant, J. C.; Millam, J. M.; Iyengar, S. S.; Tomasi, J.; Barone, V.; Mennucci, B.; Cossi, M.; Scalmani, G.; Rega, N.; Petersson, G. A.; Nakatsuji, H.; Hada, M.; Ehara, M.; Toyota, K.; Fukuda, R.; Hasegawa, J.; Ishida, M.; Nakajima, T.; Honda, Y.; Kitao, O.; Nakai, H.; Klene, M.; Li, X.; Knox, J. E.; Hratchian, H. P.; Cross, J. B.; Bakken, V.; Adamo, C.; Jaramillo, J.; Gomperts, R.; Stratmann, R. E.; Yazyev, O.; Austin, A. J.; Cammi, R.; Pomelli, C.; Ochterski, J. W.; Ayala, P. Y.; Morokuma, K.; Voth, G. A.; Salvador, P.; Dannenberg, J. J.; Zakrzewski, V. G.; Dapprich, S.; Daniels, A. D.; Strain, M. C.; Farkas, O.; Malick, D. K.; Rabuck, A. D.; Raghavachari, K.; Foresman, J. B.; Ortiz, J. V.; Cui, Q.; Baboul, A. G.; Clifford, S.; Cioslowski, J.; Stefanov, B. B.; Liu, G.; Liashenko, A.; Piskorz, P.; Komaromi, I.; Martin, R. L.; Fox, D. J.; Keith, T.; Al-Laham, M. A.; Peng, C. Y.; Nanayakkara, A.; Challacombe, M.; Gill, P. M. W.; Johnson, B.; Chen, W.; Wong, M. W.; Gonzalez, C.; Pople, J. A. *Gaussian 03*, revision C.02; Gaussian, Inc.: Wallingford, CT, 2003.
(56) Becke, A. D. *J. Chem. Phys.* **1993**, *98*, 5648−5652.
(57) Miehlich, B.; Savin, A.; Stoll, H.; Preuss, H. *Chem. Phys. Lett.* **1989**, *157*, 200−206.
(58) Lee, C.; Yang, W.; Parr, R. G. *Phys. Rev. B: Condens. Matter Mater. Phys.* **1988**, *37*, 785−789.
(59) Wadt, W. R.; Hay, P. J. *J. Chem. Phys.* **1985**, *82*, 284−298.
(60) Roy, L. E.; Hay, P. J.; Martin, R. L. *J. Chem. Theory Comput.* **2008**, *4*, 1029−1031.
(61) *X−AREA: Program for the Acquisition and Analysis of Data*, version 1.30; Stoe & Cie GmbH: Darmatadt, Germany, 2005.
(62) *X−RED: Program for Data Reduction and Absorption Correction*, version 1.28b; Stoe & Cie GmbH: Darmatadt, Germany, 2005.
(63) *X−SHAPE: Program for Crystal Optimization for Numerical Absorption Correction*, version 2.05; Stoe & Cie GmbH: Darmatadt, Germany, 2004.
(64) Sheldrick, G. M. *SHELX97. Program for Crystal Structure Solution*; University of Göttingen: Germany, 1997.
(65) Sheldrick, G. M. *SHELX97. Program for Crystal Structure Refinement;* University of Göttingen: Germany, 1997.
(66) Prince, E. *International Tables for X-ray Crystallography*, Vol *C*; Kluwer Academic Publisher: Doordrecht, The Netherlands, 1995.
(67) *X-STEP32: Crystallographic Package*, version 1.07b; Stoe & Cie GmbH: Darmstadt, Germany, 2000.
(68) Frezza, M.; Dou, Q. P.; Xiao, Y.; Samouei, H.; Rashidi, M.; Samari, F.; Hemmateenejad, B. *J. Med. Chem.* **2011**, *54*, 6166−6176.
(69) Morris, G. M.; Huey, R.; Lindstrom, W.; Sanner, M. F.; Belew, R. K.; Goodsell, D. S.; Olson, A. J. *J. Comput. Chem.* **2009**, *30*, 2785−2791.
(70) DeLano, W. L. *PyMOL*; DeLano Scientific: San Carlos, CA, 2002.

DOI: 10.1021/acs.organomet.7b00054
Organometallics XXXX, XXX, XXX−XXX